The isotope effects in RFP magnetic configuration

R. Lorenzini, M. Gobbin and RFX-mod team

Consorzio RFX, Associazione Euratom-ENEA sulla fusione, 35127 Padova, Italy

E-mail: rita.lorenzini@igi.cnr.it

Abstract. The comparison between Deuterium and Hydrogen plasmas at high current in the RFX-mod experiment proves that the Reversed Field Pinch configuration experiences the isotope effect in a way analogous to tokamak experiments.

Both energy and particle confinement exhibit a favorable scaling with the isotope mass M_i, respectively as ${M_i}^{0.3}$ and as ${M_i}^{0.45}$. This effect is mainly due to the mitigation of transport at the edge, which is driven by electrostatic fluctuations, although a mitigation of the stochastic transport in the pasma core is also observed.

As it happens in tokamaks, the MHD properties are modified when the gas mass is changed. The most evident modification regards the spectrum of tearing modes that are more stable in Deuterium, so that the duration and the purity of Quasi Single Helicity (QSH) phases are enhanced.

The thermal structures that develop during the QSH phases enclose a plasma volume that is wider in Deuterium discharges than in Hydrogen ones.

1. Introduction

The reversed field pinch (RFP) is a magnetic configuration [1, 2] alternative to the tokamak [3] on which the ITER project is based; though its development is presently at least a generation behind the Tokamak, the RFP approach to the reactor could present some attractive features, such as the weak requirements on toroidal field coil current and the possibility of reaching ignition with ohmic heating only.

The largest RFP in operation till 2015 is RFX-mod [4], with a major radius R=2m and minor radius a=0.457m. The device is presently being upgraded, modifying the magnetic front-end in order to improve its performance [5, 6]. The peculiarity of the RFP magnetic configuration is the self-sustainment of the poloidal current against the resistive decay when the applied electric field is only toroidal. This is possible thanks to a 'dynamo' poloidal electric field generated by internally resonating magnetic modes that, in particular, is responsible for the reversal of the toroidal magnetic field B_ϕ at the edge. The radius where the toroidal field changes its direction is called 'reversal radius'. The non-linear interaction of many internally resonant tearing modes with comparable amplitudes results in a Multiple Helicity (MH) state, which is the preferred plasma state at low current (for example RFX-mod plasma is in MH when $I_p < 800$ kA). The presence of such modes leads to the ergodization of the magnetic field over most of the

plasma volume and to a consequent enhancement of energy and particle transport in the plasma core. There are several evidences that the particle transport in the plasma edge is dominated by electrostatic fluctuations [7, 8] although the strong toroidal asymmetries due to the locking in phase of tearing modes constitute an additional loss channel for particle and energy [9].

From the theoretical point of view it has been shown that the dynamo field can be obtained with only one mode [10, 11] in the helical Single Helicity (SH) state. Experimental Quasi Single Helicity (QSH) states, where one mode dominates over the others (the so-called secondary ones) have been obtained in several RFP experiments [12]. Furthermore QSH states occur more and more frequently and for longer durations as the plasma current is raised [13]. The onset of a QSH is usually followed by the development of a thermal structure in the electron temperature, whose core is at the O-point of magnetic island of the dominant mode; its hot volume is enclosed by Internal Transport Barriers (eITBs), namely steep electron temperature gradients. Such thermal structures are a few centimeters wide and located off-axis when the energy of secondary modes is still high, while they become enough large to enclose the plasma core in purest QSH, when the ratio between dominant and secondary mode amplitudes increases [14].

The onset of a QSH is accompanied by an improvement of confinement in the plasma core [15, 16, 17]. Such phenomenon is mainly due to the lower magnetic field stochastization, which results from the reduced amplitude of secondary modes, combined to the increased resilience of helical states to magnetic chaos [18] with respect to the axisymmetric ones. The transport at the edge in spontaneous QSH states is also believed to be dominated by electrostatic fluctuations, although it has not be proven experimentally since the high level of currents prevents the use of probes.

The experimental results on the isotope effect on MHD, energy and particle transport in RFX-mod are described in [19], while the isotope effect on spontaneous and induced ITBs is presented in [20], where the isotope effect is also investigated through a Hamiltonian guiding center code simulations. Here we present a review of main results.

RFX-mod has been operated in Hydrogen since its beginning up to 2014, when the Hydrogen has been replaced with Deuterium. The operations in Deuterium lasted until the end of 2015 when the machine has been shut down. Due to the outflux of the Carbon first wall, the plasmas obtained in such Deuterium campaign are actually a mixture of about 40% of Hydrogen and about 60% of Deuterium.

The Deuterium campaign has been devoted mainly to the exploration of high current regime (Ip $\sim$ 1.5 MA), which favours the formation of spontaneous electron transport barriers during the QSH phases. This result is conditioned to the good control of the radial magnetic field at the edge obtained through a sophisticated system of 192 feedback controlled saddle coils [21, 22].

Since the isotope effect studies have been performed comparing high current discharges in H and in D they regard the RFP physics in QSH regimes.

It results that, also in a Reversed Field Pinch, the main ion mass has an impact on the MHD phenomena and on plasma confinement. As in tokamaks, discharges with the same external settings perform better in Deuterium than in Hydrogen.

In the following the isotope effect on several aspects of RFP plasma physics is described: the behavior of tearing modes, with particular emphasis to Quasi Single Helicity regimes, is presented in Section 2, while the sawtoothing dynamics is described in Section 3. The energy confinement and the ITBs behaviour are discussed in Section 4 and in Section 5.

The first part of Section 6 discusses the particle confinement and influx, while the second part describes particle transport simulations. Finally in Section 7 we draw the conclusions.

2. Isotope effect on tearing modes in QSH

In this paper we present a comparison between Deuterium and Hydrogen RFP plasmas at high plasma current ($I_p \sim 1.5$ MA) in RFX-mod. At this level of current, with an appropriate tuning of discharge parameters, the plasma stays preferentially in QSH state [23, 24].

A QSH develops when the plasma is kept in a particular equilibrium called 'shallow' reversal equilibrium since it is characterized by a low reversed B_ϕ at the wall. The reversal of an RFP equlibrium is quantified by the reversal parameter $F = B_\phi(a)/ < B_\phi >$, where $< B_\phi >$ is the toroidal field averaged on the poloidal section. A shallow equilibrium, like the one of the Deuterium shot 35050 shown in Fig. 1c, has F > -0.03. In addition QSH are obtained when the Greenwald fraction n/n_G, defined as the density normalized to the Greenwald density $n_G = I/(\pi a)$, is lower than about 0.3.

The tearing mode that in QSH dominates the spectrum of the m=1 modes (m being the poloidal mode number) has toroidal number n=-7 in RFX-mod (black time trace in Fig. 1b), and it is the innermost resonant one, as usually happens even in the other RFP experiments.

The amplitude of dominant and secondary m=1 modes can be combined to evaluate the spectral index N_s that quantifies the purity of the spectrum:

$$N_s = \left[\sum_{j=-23}^{-7} \left(\left(b_\phi^{1,j}\right)^2 / \sum_{j=-23}^{-7} \left(b_\phi^{1,j}\right)^2 \right)^2 \right]^{-1} \quad (1)$$

where $b_\phi^{1,j}$ are the toroidal harmonics measured at the plasma edge. The lowest value $N_s = 1$ is achieved only in the pure SH regime, hence a N_s value progressively decreasing, as it happens for example when the plasma current is raised, indicates that QSH states are approaching the ideal Single Helicity.

In this paper the plasma is considered to be in QSH when N_s is lower than 2.

As a general remark the comparison between Deuterium and Hydrogen discharges shows that Deuterium QSH is closer to SH, in particular when n/n_G is greater than 0.1

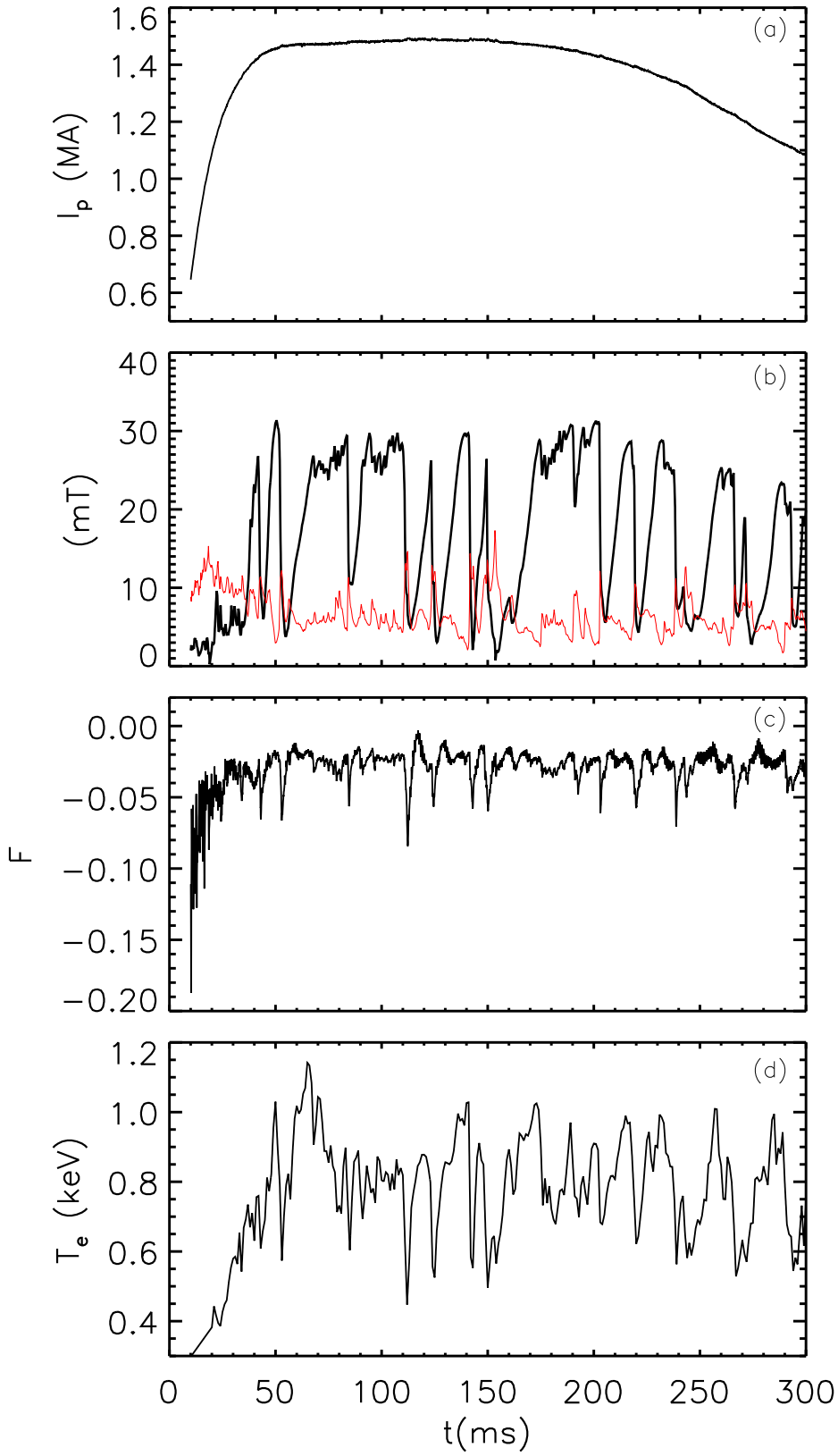

Figure 1. Time traces of current (a), dominant mode amplitude (in black) and cumulative amplitude of secondary modes (in red) measured at the edge (b), F parameter (c) and core electron temperature (d). These time traces belong to the Deuterium discharge 35050

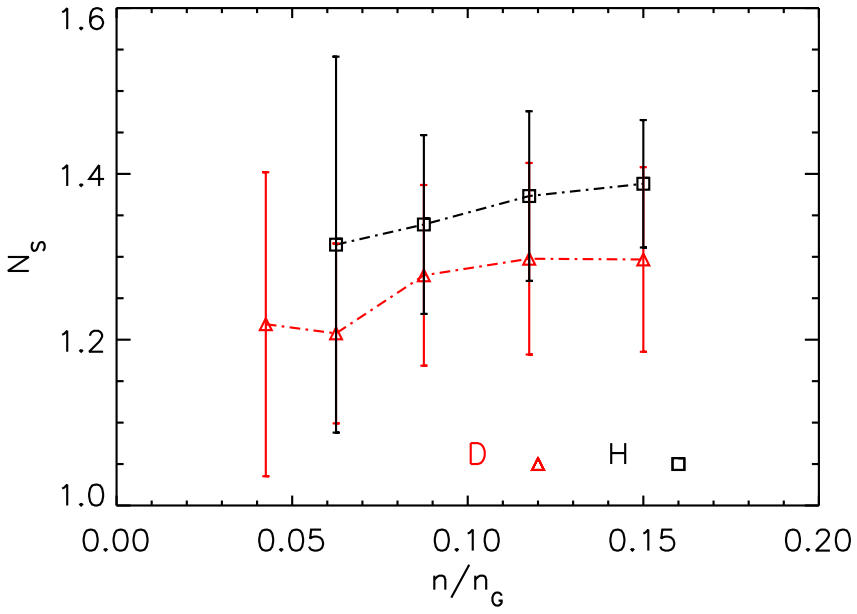

Figure 2. Comparison between the spectral index N_s of D and H similar discharges: the values are averages of measurements taken during QSH phases

as shown in Fig. 2. The plot of N_s, as well as all the plots involving average data from here ahead, refers to QSHs lasting at least 2 ms.

The value for the Hydrogen $n/n_G \leq 0.05$, obtained in Deuterium with $n_e \leq 1 \cdot 10^{19} m^{-3}$, is missing in the plot since such a low density regime was never achieved.

The amplitude of the dominant mode and the cumulative amplitude $b_{\phi,sec}$ of secondary modes have been compared to understand which of them plays the leading role in the lowering of N_s:

$$b_{\phi,sec} = \sqrt{\sum_{j=-23}^{-8} (b_\phi^{1,j})^2} \tag{2}$$

Such analysis leads to conclude that, as shown by the comparison between the plot 3a and 3b, the leading role is played by the secondary modes whose spectrum changes as a result of the different isotope mass. However the normalized amplitude of the dominant mode in D and H is similar, leading to conclude that the amplitude of the dominant mode is unaffected by the mass of main gas.

According to the simulations performed with the NIMROD code presented in [25] the stabilizing mechanism could be found in a first order finite Larmor radius FLR effect on MHD instabilities.

Typically QSH states have an oscillatory behavior, since the plasma comes back to the MH state during the periodic Discrete Relaxation Events (DRE) [26], when the toroidal flux is self-generated in a discrete way by the dynamo [27]. During such events the destabilization of m=1 modes follows a cascading process that starts from the

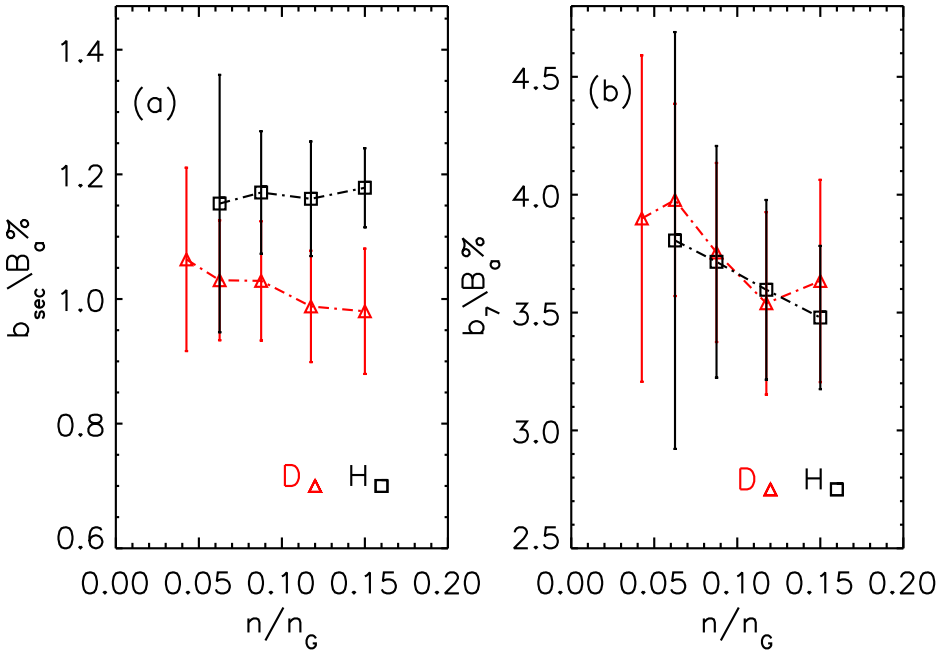

Figure 3. Comparison of secondary mode amplitude (a) and dominant mode amplitude (b) in Deuterium and Hydrogen shots: the values, plotted versus the Greenwald fraction, are averages of measurements taken during QSH phases.

innermost resonant harmonics and propagates to the outer ones in a few milliseconds. The last phase of a DRE is the destabilization of the m=0 modes, which regenerate the toroidal magnetic flux as indicated by the negative peaks of F shown in Fig. 1c. Following the DRE the secondary mode amplitude rapidly decreases and the plasma regains the unperturbed state.

The duration τ_{QSH} of QSH phases is affected by the choice of the main gas. In fact in the low density range $n/n_G \leq 0.1$ τ_{QSH} is almost twice longer in Deuterium than in Hydrogen as shown in Fig. 4. This result is the second indication that the increase of isotope mass M_i brings the still periodic QSH closer to the stationary SH.

A deeper insight into this phenomenon can be obtained comparing the probability density function of τ_{QSH} obtained for both gases at $n/n_G \leq 0.1$.

As it can be seen in Fig. 5 the pdf of Deuterium is shifted towards larger values and includes $\tau_{QSH} > 20$ ms that in Hydrogen have never been recorded.

The probability decreases dramatically for $\tau_{QSH} > 40$ ms because such long QSHs, lasting as long as the current flat top, are difficult to obtain.

3. Isotope effect on Dynamo Relaxation Events

The DREs are not a peculiar characteristic of QSH state since they have been observed also in MH plasmas [28].

However in the RFX-mod large DREs are usually observed, as a result of the lower

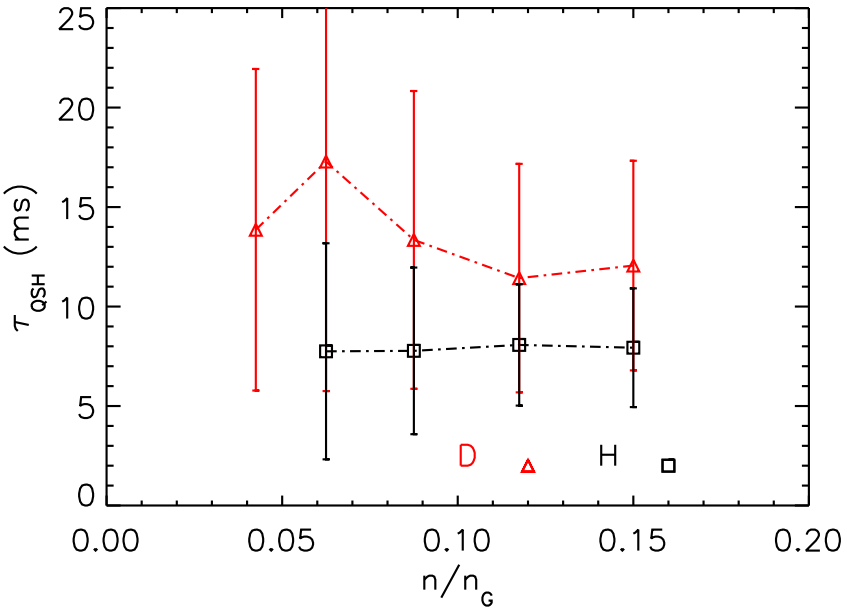

Figure 4. Comparison of QSH duration in D and H discharges.

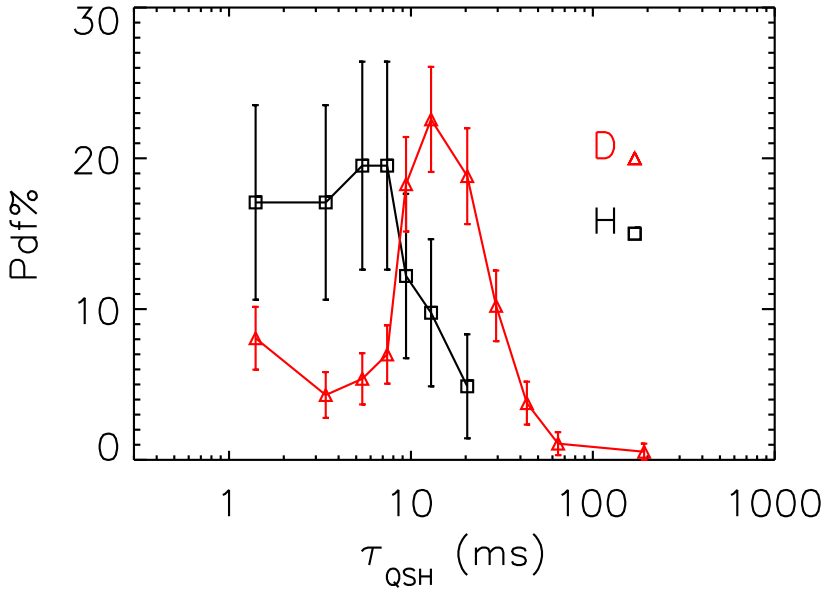

Figure 5. Comparison between the probability density function of τ_{QSH} calculated in the low density regime of Deuterium and Hydrogen discharges

shell-plasma proximity b/a (where b is the shell radius while a is the plasma radius) that has been changed from 1.24 to 1.1, and of the active control system, which mimics a perfect conducting shell. This is similar to what happens in MST [29] that is the RFP machine with the lowest shell-plasma proximity (b/a=1.04).

Moving from H to D some aspects of the Discrete Relaxation Events physics modify as shown by the distribution of DRE strength in Fig. 6. The DRE strength is defined as the F deepening $\Delta F = F_{DRE} - < F >$, where the symbol $<>$ means the average over some milliseconds before the DRE occurrence.

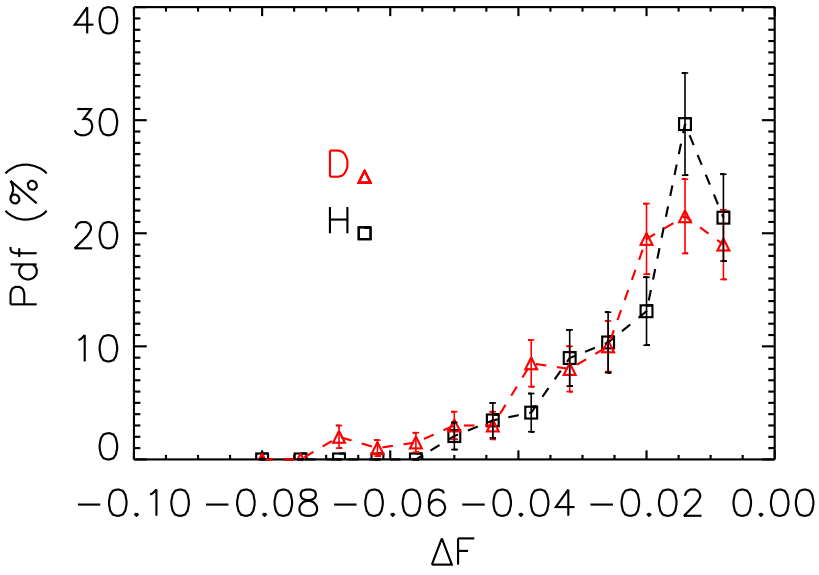

Figure 6. Comparison between the pdf of DRE ΔF in Deuterium and Hydrogen

The comparison between the probability density functions shows that in H plasmas smaller DREs ($\Delta F > -0.2$) are more likely than in the Deuterium ones; furthermore DREs with $\Delta F < -0.05$ are observed only in Deuterium.

In tokamak experiments the sawtoothing slows down in D plasma; this happens in RFPs too, but the interval between consecutive DREs increases by only 1 ms in Deuterium with respect to the average value of about 6 ms in Hydrogen.

However such effect is too small (only 15%) to explain the two times increase, shown in Fig. 4, of QSH duration observed in Deuterium, which is likely due to a greater resilience of Deuterium QSH to the occurrence of DRE. The data analysis shows that 75% of DREs make a QSH crash in Hydrogen plasma, while this percentage reduces to 55% in the case of Deuterium. To go into deeper details about the relationship between the DREs occurrence and QSH crash the pdf of ΔF of DREs that make the QSH crash (DRE_{crash}) has been calculated.

As it happens for the pdf of all the DREs, the pdf of DRE_{crash} group is shifted towards stronger ΔF in Deuterium (see Fig. 7), as it could be expected since the strongest DREs with $\Delta F < -0.05$ are always associated to a QSH crash.

The comparison between the probability density functions of DRE_{crash} with $\Delta F > -0.02$ indicate that their difference cannot be explained only in terms of the lower

probability of weak DRE shown in Fig 6. However this difference is mainly due to the greater resilience of QSH state to weak DREs in Deuterium discharges.

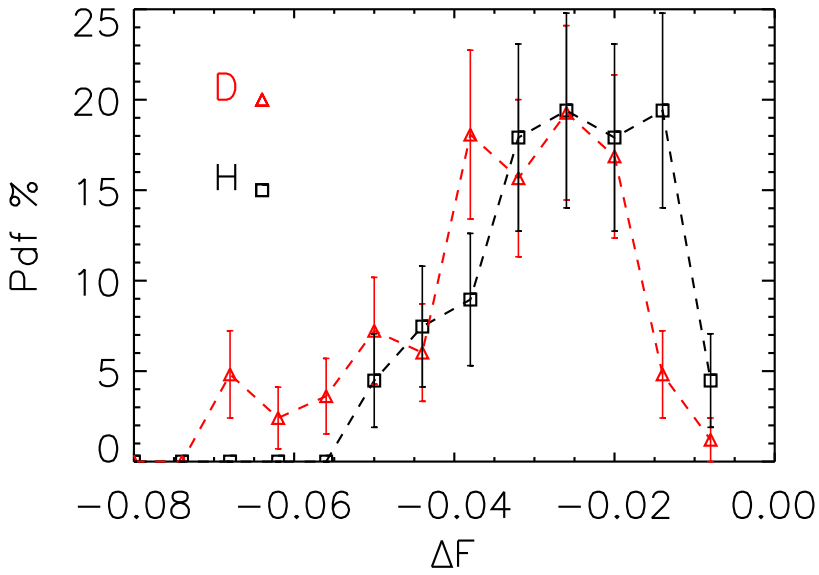

Figure 7. Comparison between the probability density function of DRE_{crash} strenght calculated in Deuterium and Hydrogen

4. Isotope effect on energy transport and confinement

The core electron temperature T_e is measured in RFX-mod by a double filter system with sampling frequency of 1 kHz. The core radial T_e profile is measured with a 84-point Thomson Scattering (TS) diagnostics [30] in a broad fraction of the plasma radius ($0 < r/a < 0.87$) with a time resolution of 10 ms. The profile at the edge is measured with a Thermal Helium Beam (THB) diagnostics [31] in the region $0.94 < r/a < 1$ with a spatial resolution of 5 mm and a temporal one of 3 ms. These measurements are complemented by the data of a multi-chord, double filter SXR spectrometer with a high sampling frequency (up to 10 kHz) [32], which will be described in a greater detail in the final part of this Section.

Fig. 8, where the averaged temperatures are plotted versus the Greenwald fraction, shows that the core temperature of Deuterium plasmas is higher by about 150 eV with respect to Hydrogen plasmas, and that such effect is more evident when the Greenwald fraction is higher than 0.1. This result is in line with the mitigation of transport expected on the basis of reduced amplitude of secondary modes shown in Section 2, since tearing modes play a crucial role as drivers of energy transport in the core [32, 33]. If they are big enough, the magnetic islands of such modes overlap making the field stochastic and

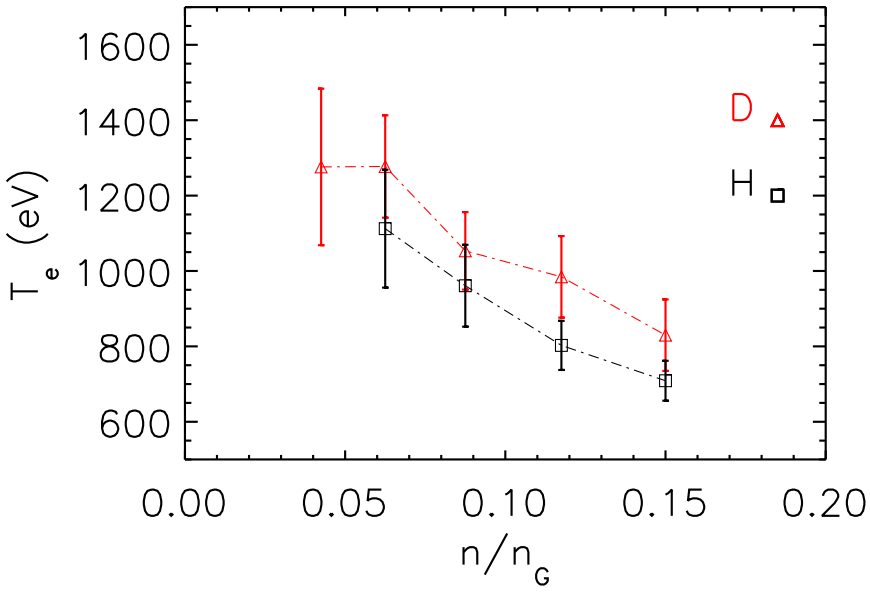

Figure 8. Comparison between core electron temperature measured during QSH in Hydrogen and Deuterium

enhancing the transport. Such effect is lower in QSH since the magnetic islands, whose size is related to the amplitude of modes, are smaller than in MH.

The modification of T_e profile induced by the isotope effect has been studied using data of the space resolved diagnostics TS and THB. The profiles included in the ensamble averages have been measured during QSH of similar discharges, and do not exhibit strong HFS/LFS asymmetries related to the presence of off-axis thermal structures [18]. An example of the obtained ensamble average is plotted in Fig. 9a; the profiles are measured in shots at $0.1 < n/n_G < 0.13$, which is the density interval where the highest number of profiles has been collected.

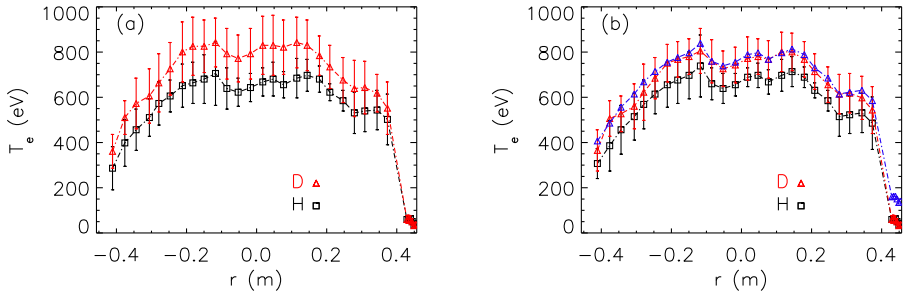

Figure 9. Electron temperature average profiles in the density range ($0.1 < n/n_G < 0.13$). (a) data are measured during QSH in similar discharges. (b) data are taken during the QSH of similar discharges having analogous values of secondary modes. The blue line is obtained adding to the Hydrogen profile a constant value of about 100 eV

The analyses of radial profiles measured during QSH confirms that the core temperature is higher in Deuterium plasmas than in Hydrogen ones. The difference of about 170 eV supports the results obtained with double filter diagnostics. Fig. 9a shows that the isotope effect induces two different modifications in the T_e profile. As expected from the reduction of secondary modes the core gradients (r $<$ 0.3 m) in Deuterium are slightly steeper than in Hydrogen.

However a second effect is also evident in the external region of the plasma, since T_e of Deuterium plasmas maintains higher up to r $\sim$ 0.4 m. Such effect is lost in the more external region (r $\geq$ 0.43 m), where the THB measurements relatives to the two main gases overlap. The higher steepness of Deuterium gradient in the edge region 0.4m $<$r $<$ 0.43m demonstrate that the isotope effect has a beneficial influence even on the electrostatic channel of the trasport [34]

To isolate the influence of the reduced core stochastic transport of D plasma on T_e profile a second class of average profiles has been calculated, using only profiles that have similar operational parameters (like plasma current, density and reversal parameter) and that share the value of amplitude of secondary modes (averaged on a time interval of 0.4 ms at the time of TS measurements).

Although the value of cumulative mode amplitude of D shots is typically lower than the value of analogous H shots, in the density range $0.1 < n/n_G < 0.13$ used in Fig. 9a it has been possible to find a sufficiently wide database to make a comparison.

It can be seen from Fig. 9b, where we plotted the profiles obtained in this second case, that, while the difference between the temperatures of two gases is still present up to r $\sim$ 0.4 m, the difference between the core gradients does not hold anymore. In fact the blue profile, obtained adding to the Hydrogen profile a constant value of about 100 eV, almost overlaps the Deuterium profile at r$<$0.4 m. We conclude that the lowering of secondary modes, which makes steeper the core gradients, is only partially responsible of the isotope effect on the electron temperature. 60% of the difference between the two profiles comes from the enhancement of T_e in the pedestal region (0.4m $<$ r $<$ 0.43 m), due to the mitigation of a transport mechanism of electrostatic nature.

As it occurs during a sawtooth in tokamaks the enhancement of energy transport induced by a DRE lowers the core electron temperature, as shown in Fig. 1d. Such effect is studied analyzing the difference ΔT_e between the temperature measured during the relaxation event T_e^{DRE}, and the unperturbed temperature T_e^{bef} measured immediately before the crash. T_e^{bef} is calculated averaging T_e on a interval of 2 ms just before the starting of the relaxation process, while T_e^{DRE} is the average of T_e in an interval of 2 ms which includes the phase of maximum F deepening. The averages are calculated in discharges with analogous external settings.

In Fig. 10 ΔT_e is plotted versus the spectral index calculated during the DRE $N_{s,DRE}$; the log scale of the ascissa emphasizes that, when $1 < N_{s,DRE} < 2$, QSH survives the DREs, while if $N_{s,DRE} > 2$ the plasma looses the QSH during the DRE and enters the MH. The decrease of core temperature is lower when the discrete generation of toroidal flux happens during a QSH. This is true for both Deuterium and Hydrogen

plasmas, where an analogous value of $\Delta T_e \sim 150eV$ is found.

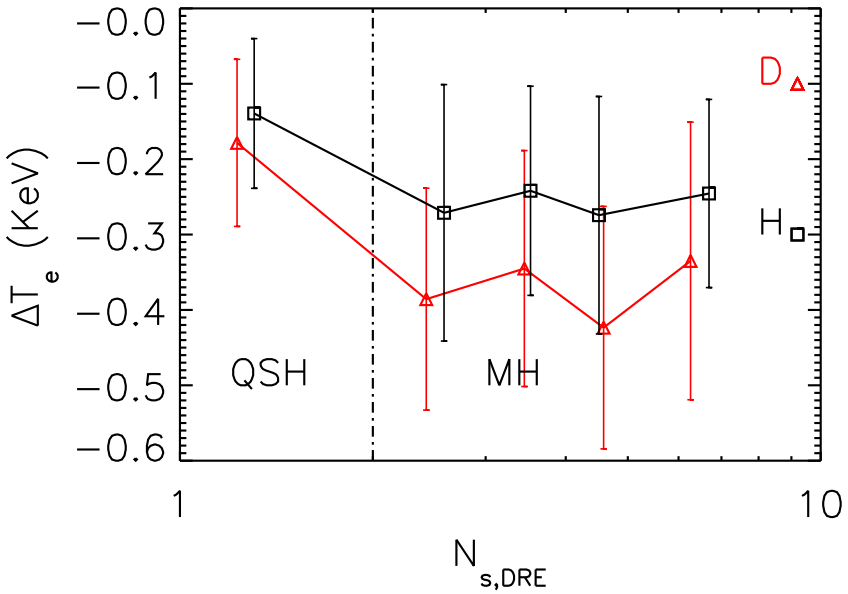

Figure 10. Comparison of the core temperature decrease ΔT_e due to a DRE occurrence in Hydrogen and Deuterium.

When QSH evolves in MH ($N_{s,DRE} > 2$), the temperature decreases by about 250 eV in Hydrogen, while the T_e drop reaches values of about -350 eV in Deuterium, independently on the final value of $N_{s,DRE}$. The drop ΔT_e in Deuterium is $\sim 150eV$ higher than the drop in Hydrogen. This means that the difference in the core temperature between H and D that is measured in QSH is lost during the relaxation event, and the isotope effect does not hold anymore. Instead, when the DRE occurs in QSH, since ΔT_e has an analogous value in both gases, the isotope effect is maintained during the relaxation event.

The energy confinement time τ_E is calculated assuming that the ion temperature T_i is $\sim 0.7\ T_e$ [13], since no measurements of T_i were available during the Deuterium campaign. As expected considering that the ohmic input power is similar in both main gases, the behaviour of confinement time τ_E reminds that of T_e, as shown in Fig. 11.

The energy confinement times scales with the mass M_i of the isotope with the highest concentration as $\tau_E \sim M_i^{0.3}$, with the exception of low density regimes ($n/n_G < 0.08$) where the weaker dependence $\tau_E \sim M_i^{0.15}$ is found. τ_E scaling in RFP shows a weaker dependence on the ion mass than in tokamak ohmic regimes where $\tau_E \sim M_i^{0.5}$. However it should be considered that the ohmic regimes in tokamak benefit of a supplementary effect on the input power [35, 36]. When only the intrinsic effect of confinement improvement is considered, the tokamak scaling becomes $\tau_E \sim M_i^{0.35}$, more similar to the RFP case.

The low time resolution of the Thomson Scattering diagnostic prevents to follow

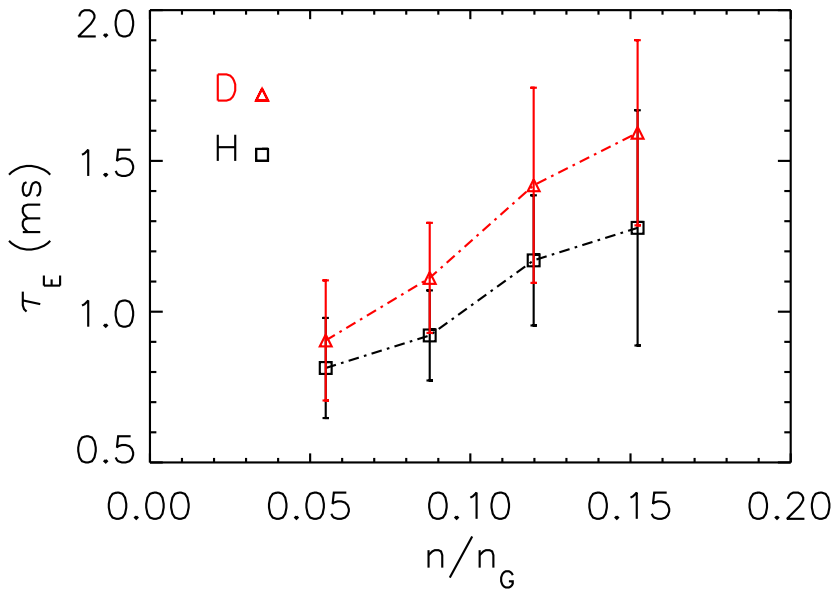

Figure 11. Comparison of τ_E found in Deuterium and Hydrogen plasma. The values are estimated from TS profiles.

in detail the fast dynamic of the internal electron transport barriers. For this reason the time evolution of ITB is studied through the data collected by the Diagnostic Soft X-rays at 3-arrays (DSX3) tomography [32]; indeed this diagnostic, which exploits the two-foil technique [37] to reconstruct the maximum electron temperature along 19 lines of sight, is characterized by a high temporal resolution ($\sim 6kHz$). Despite the drawback of a lower spatial resolution ($\sim 6cm$) with respect to the Thomson scattering, it allows a good characterization of the T_e gradient evolution in the core region of the plasma. In particular the data used here amount to a total of about 10000 electron temperature profiles measured during helical states relative to ~ 80 discharges, half in Hydrogen and half in Deuterium with the following parameters: $I_p = 1.4 - 1.6$MA (only flattop phase), $n_e = 1 - 4 \cdot 10^{19} m^{-3}$ and $-0.025 \leq F \leq -0.015$.

The T_e data from DXS3 are generally plotted as function of the distance of the lines of sight from the plasma center (i.e. the impact parameter p) normalized to the minor radius a. Fig. 12 shows a couple of examples: in panel a the plasma core electron temperature at $p/a = 0.1 - 0.5$ is almost constant with values up to $\sim 0.9 - 1$ keV and a clear eITB is visible around $p/a = \pm 0.5$; in (b), the profile is always below 0.85keV with a flat area extending over most of the radius ($-0.5 < p/a < 0.45$) and reduced gradients.

The characterization of the DSX3 T_e profiles is performed by means of two quantities: the gradient magnitude (∇T_e) and the width of the thermal structure Δ_{str}. The former can be evaluated by a mobile linear fit [32] over a maximum of 10 data points and provides an estimate of the maximum gradient ∇T_e (within an error of 0.4 keV/m)

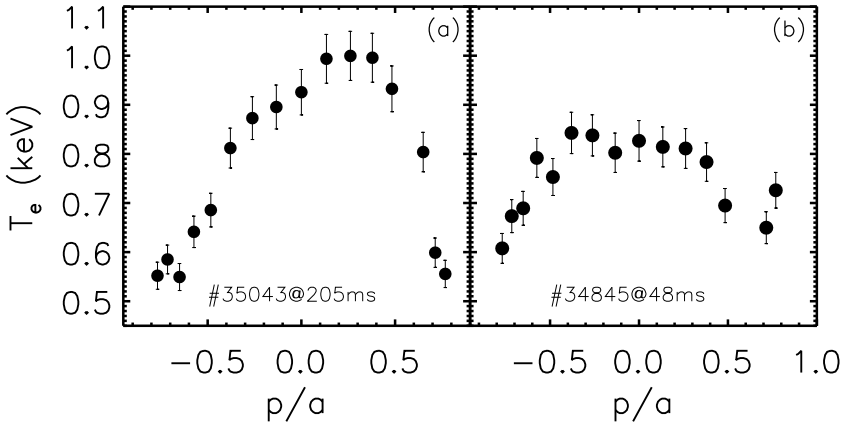

Figure 12. Two examples electron temperature from DSX3: (a) steep gradients sustain a flat central region (Deuterium discharge); (b) an almost flat T_e profile with low gradients (Hydrogen discharge).

and of its position i.e. the location of the transport barrier which corresponds to a region with vanishing magnetic shear. Indeed, as reported in [38], helical RFP plasmas are characterized by a non monotonic safety factor profile going through a maximum located in the vicinity of the electron transport barriers. On the other side, the thermal structure width Δ_{str} describes the region of the plasma having an electron temperature close to its maximum value and has been defined considering the impact parameters where $T_e \geq 3/4T_{e,max}$: the minimum and maximum of them are labeled respectively as $(p/a)^-$ and $(p/a)^+$. Then:

$$\Delta_{str} = \frac{(p/a)^+ - (p/a)^-}{2} \tag{3}$$

Note that Δ_{str} is a quantity normalized to the minor radius a.

The DSX3 allows to evaluate these two parameters every $0.5ms$; an example of the gradient time evolution with other quantities of interest is shown in Fig.13. In particular Fig. 13a reports the electron temperature from two lines of sight with impact parameters corresponding to the inner (black, $@p/a \sim 0$) and outer (red, $@p/a \sim 0.7$) region of the plasma while panel c shows the magnetic modes amplitude (dominant in black, secondary ones in red). The associated dynamic of the maximum temperature gradient measured by the DSX3 diagnostic is displayed in panel b: ∇T_e oscillates from 1 to 5keV/m with higher values generally corresponding to the rising or flattop phase of the dominant mode. Panel d of the same figure shows the ∇T_e distribution corresponding to discharges in Deuterium (red) and Hydrogen (black) during magnetic helical states. For both the isotopes the maximum of the distribution falls close to $\nabla T_e \sim 1.5$ keV/m, thus such a value has been used as separator between flat and steeper T_e profiles. It is worth to note that the distributions are very similar for both the gases as could be expected following the considerations in Section 4 which pointed out how the higher

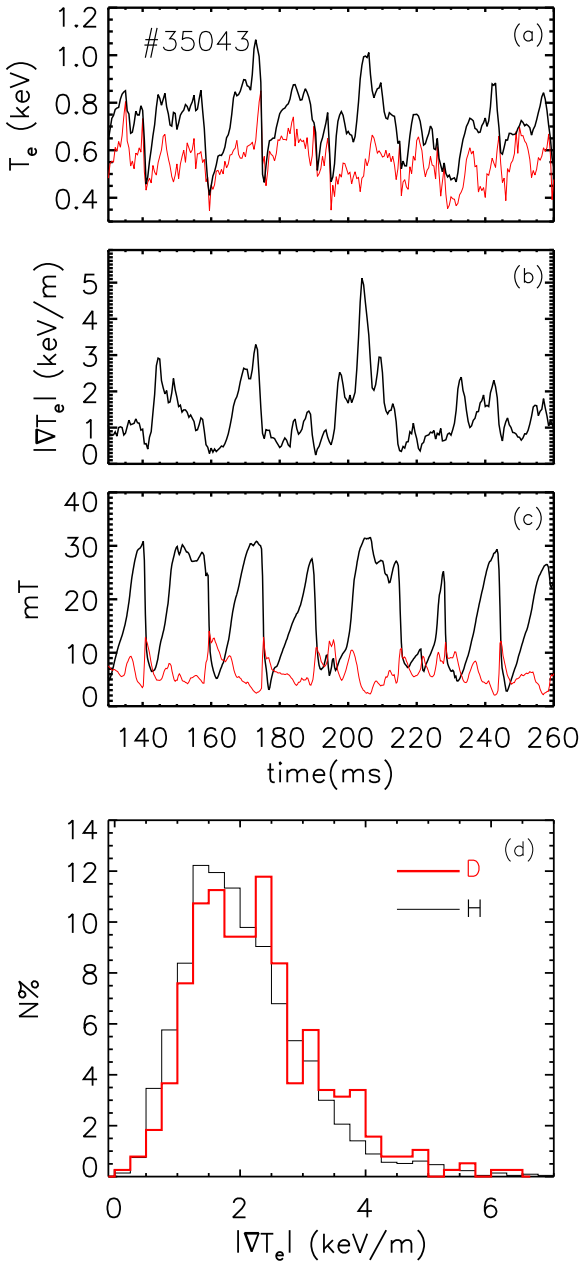

Figure 13. Time evolution for: (a) core (black) and outer electron temperature (red), (b) maximum temperature gradient ∇T_e from DSX3 and (c) dominant (black-thick line) and secondary modes (red thin line). In (d) the distribution for the T_e gradients is reported both for hydrogen (black) and deuterium (red) discharges.

values of T_e in D plasmas are related with different properties at the pedestal near the edge rather than to features of the core/mid region.

Concerning the parameter Δ_{str}, it generally varies from values greater than 0.4, typical of thermal structures extending over a relevant portion of the plasma (for instance the one in Fig. 12a), to lower than 0.35 which characterize T_e profiles with only a small region at high temperature. Fig. 14 reports the averaged parameters Δ_{str} and ∇T_e of eITBs ($\nabla T_e > 1.5$ keV/m) as function of n/n_G. In order to exclude transient eITBs, generally developing during the rising phase of the dominant mode-, the database has been limited to phases where $N_s < 1.6$. Fig. 14a confirms what already described in Fig.13d with similar values of ∇T_e in H and D plasmas within error bars. The same conclusion hold also for Δ_{str} shown in Fig. 14b, except at low density around $n/n_G \leq 0.15$ where $\Delta_{str} \approx 0.45$ in D and 0.38 in H. Such a behavior is probably related to the lower secondary modes level typical of D plasmas which corresponds to a larger dimensions of the thermal structures, as reported also in [14].

The same condition $N_s < 1.6$ has been imposed to analyze the duration of the eiTB i.e. the time during which $\nabla T_e > 1.5 keV/m$ for each QSH period not interrupted by back transitions to a MH topology. Fig. 15a reports the fraction of a QSH cycle characterized by the occurring of eITBs vs n/n_G. The plot shows that the development of eITBs decreases from 60% at $n/n_G \leq 0.1$ to only 20% at larger densities ($n/n_G \geq 0.3$) with similar values for the two isotopes within the error bars. Concerning the comparison between the consecutive time periods with $\nabla T_e > 1.5$ keV/m, reported in Fig. 15b, only around $n/n_G \sim 0.2$ the value of $t_{\nabla T_e}$ is partially greater by $1-2$ms in Deuterium than in Hydrogen.

5. Isotope effect in plasma with helical boundary conditions by 3D fields application

The transition to helical states can be stimulated by means of 3D fields generated by active coils as already reported from experiments not only in RFX-mod [39] but also in other RFP devices like EXTRAP T2R [40]. RFX-mod is particularly suitable for these studies thanks to its advanced system of 192 feedback saddle coils for the control of MHD instabilities which has allowed to improve the plasma confinement and stability properties. While in standard operations [41] the system tries to zero the radial field of all the poloidal/toroidal harmonics (m, n) at the edge, the sustainment of QSH states can be favored by relaxing this condition for the dominant mode harmonic amplitude $(1, -7)$ which is set at reference value $b^{1,-7}_{r,ref}(a) \neq 0$. In other words magnetic feedback allows to force the plasma boundary to a helical deformation with the selected helicity. Dedicated experiments have been performed to analyze the impact of the non zero reference for the dominant mode on the generation and persistence of the eITB both in Hydrogen and Deuterium discharges. To this end several reference amplitudes have been considered: $b^{1,-7}_{r,ref}(a) = 1 - 8$mT, i.e. about the $0.2 - 1.6\%$ with respect to the magnetic field at $r = a$. A scan has been also performed in terms of the rotation frequency of the

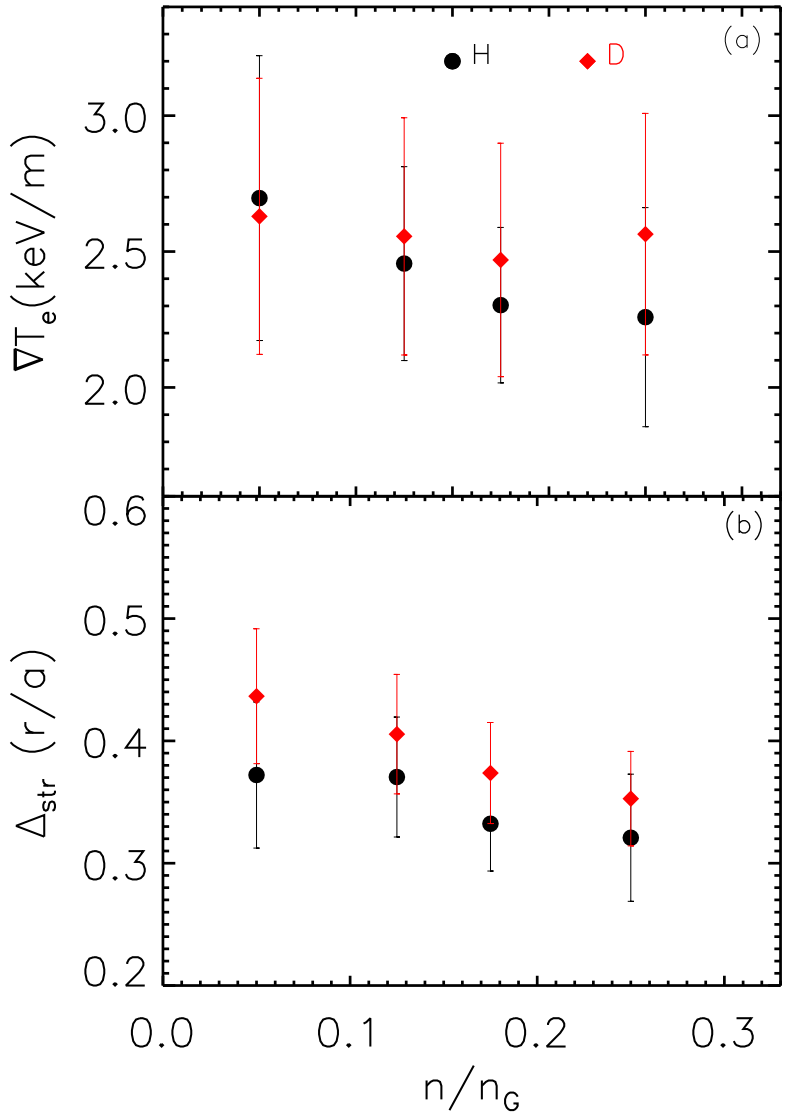

Figure 14. (a) Electron temperature gradient and (b)thermal structure size Δ_{str} in standard Hydrogen (black circles) and Deuterium (red diamonds) plasmas averaged over different classes of the Greenwald fraction n/n_G.

mode ($f = 0, 20, 30$ Hz).

An example of 3D field application is reported in Fig. 16 with $b^{1,-7}_{r,ref}(a) = 8mT$ in the interval $50 - 150$ms for a Deuterium discharge. Fig. 16b, reporting the modes evolution, shows that the dominant one never decreases to low values ($b_{1,-7}/B(a) \geq 3\%$) despite partial crashes might occur. In this case the applied perturbation is also rotating at a frequency of $f = 20Hz$ (panel c). The increase of the secondary modes, during the temporary interruptions of the dominant one, can partially enhance the residual stochasticity and affect the confinement properties of the plasma and, in particular, the

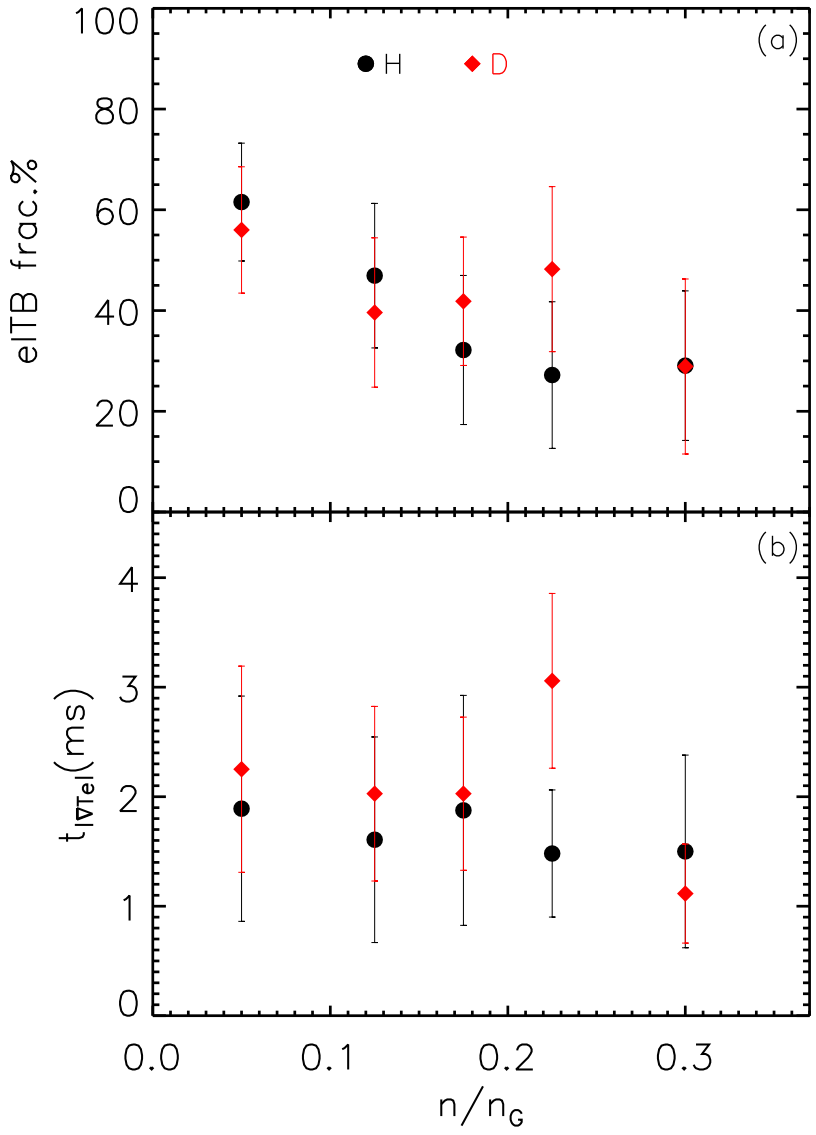

Figure 15. (a) eiTB over QSH duration and (b) consecutive eITB periods in standard Hydrogen (black circles) and Deuterium (red diamonds) discharges averaged for different classes of the Greenwald fraction.

strength of the temperature gradient. For this reason a longer duration for the helical magnetic topology might not correspond to a higher persistence of the eITBs. Such an issue has been investigated over a large database using the T_e data from DSX3 and with similar analysis to those reported in the previous section.

The distributions of $|\nabla T_e|$ during QSH phases in D and H discharges with $b^{1,-7}_{r,ref}(a) \neq 0$, reported in Fig. 17a, clearly evidence a shift between the data for the two gasses, and in particular for the values relative to the maxima (at $\sim$ 2keV/m for D and $\sim$ 1.5keV/m for H). It is worth to note that with respect to standard discharges, without 3D fields

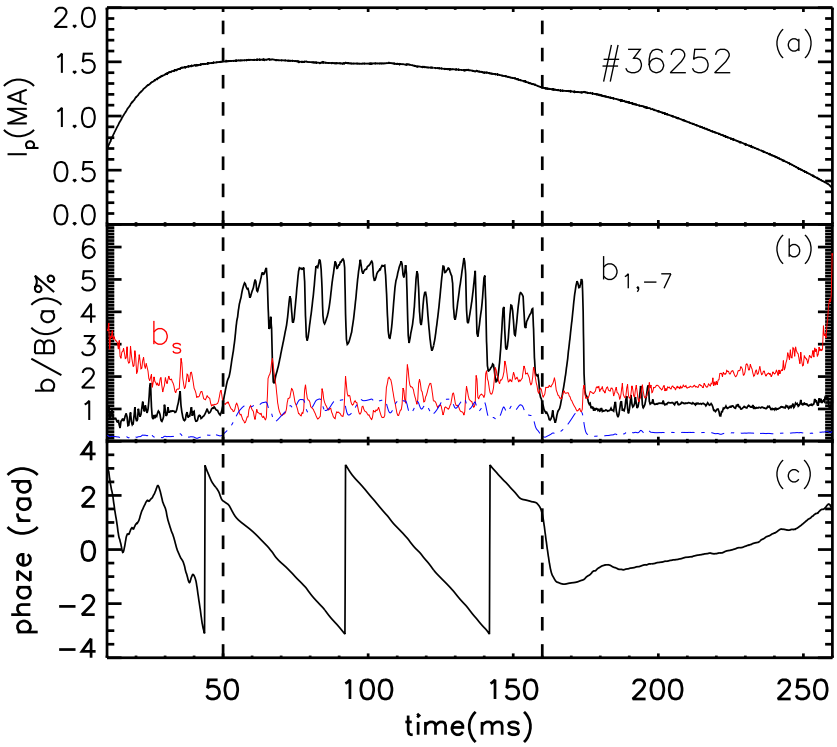

Figure 16. Helical boundary conditions applied during a Deuterium discharge: (a) plasma current; (b) normalized dominant (black)-secondary modes (red) evolution; in blue the radial field for the dominant mode $(1, -7)$ imposed by the control system (measured at the edge); (c) phase of the dominant mode. The non-zero $(1, -7)$ perturbation is applied between the two dotted vertical lines.

application, on one side the maximum for Deuterium is greater and also more cases fall in the interval $4 - 6$keV/m relative to steeper gradients, on the other side no relevant different are observed for Hydrogen. The larger $|\nabla T_e|$ values observed for D in shots with helical boundary conditions and their persistence strongly depend on the density as shown in the panels reporting the averaged values for different classes of n/n_G. The fraction of time with eITB, indeed, decreases from $\sim 60\%$ to $\sim 20\%$ when n/n_G is in the range $0.15 - 0.3$, with similar values in both gases. Nevertheless, at $n/n_G \leq 0.1$, the eITB fraction for Deuterium is higher than in Hydrogen also within error bars. A similar behavior is observed also at very large densities $n/n_G = 0.3$ but needs to be further investigated in future dedicated campaigns increasing the statistics. The core electron temperature, as in standard discharges, is generally higher in Deuterium with respect to Hydrogen but such a difference ($\sim +0.25keV$), as shown in Fig. 17c, is still larger when 3D fields are applied and occurs at all densities. On the contrary the average steeper electron gradient for deuterium plasmas, in panel 17d, is mainly associated to those profiles at $n/n_g = 0.05$ and in the interval at $0.15 - 0.20$ i.e. they are the ones

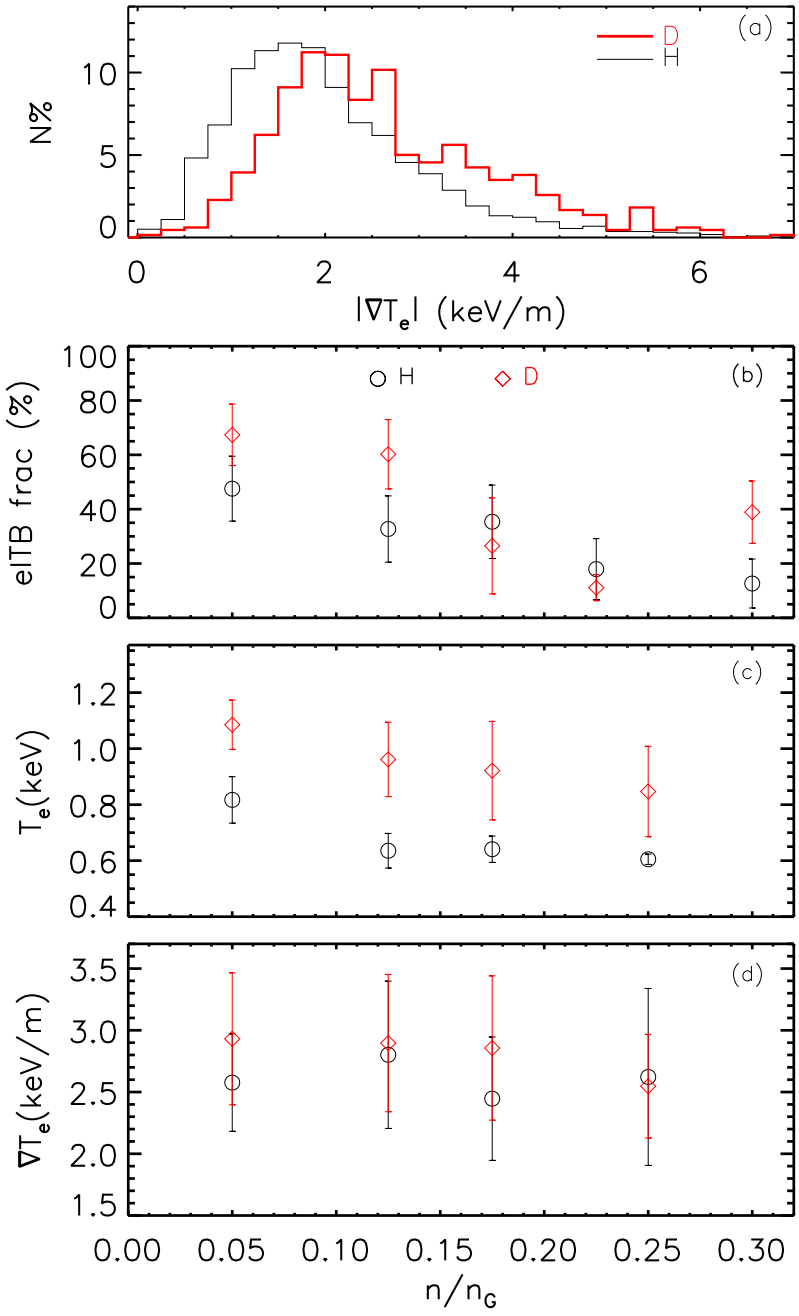

Figure 17. (a) Statistical distribution of the electron T_e gradient for Hydrogen (black) and Deuterium (red) with non zero reference for the dominant mode; (b) average ratio of eITB duration over QSH cycle period for Hydrogen (black-circles) and Deuterium (diamonds-red) with helical boundary conditions vs n/n_G. Average electron temperature in the core (c) and (d) temperature gradient for different classes of n/n_G.

which most contribute to the different distributions described in Fig. 17a.

The dependence of the main quantities of interest on $b^{1,-7}_{r,ref}(a)/B(a)$ has been

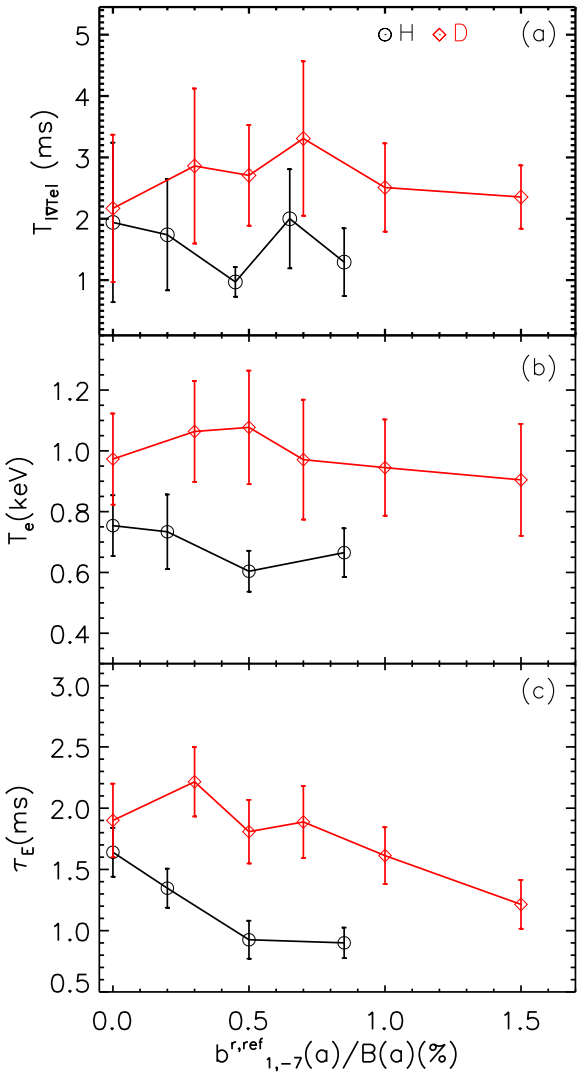

Figure 18. (a) Consecutive eITB periods (b) core electron temperature and (c) confinement time averaged for more classes of $^{1,-7}_{r,ref}(a)/B(a)$ in Hydrogen (black circles) and Deuterium (red diamonds) plasmas.

analyzed in the density range $0.05 < n/n_G < 0.2$ where similar amplitudes of the reference dominant perturbation have been applied both in Deuterium and Hydrogen plasmas. The results are reported in Fig.18 and show the average ratio between the eITB persistence with respect to QSH duration (a), the average core T_e from DSX3 diagnostic (b) and the confinement time τ_e (c) as function of the externally imposed amplitude $b^{1,-7}_{r,ref}(a)/B(a)$. While an impact of helical boundary conditions on the eITB persistency is not observed for Hydrogen, on the contrary it slightly increases for Deuterium of more than $1ms$ with a maximum at $b^{1,-7}_{r,ref}(a)/B(a) = 0.8\%$. An analogous trend holds also for the core temperature: while in Hydrogen it decreases at higher amplitude of $b^{1,-7}_{r,ref}(a)/B(a)$, in Deuterium it varies from ~ 0.9keV in standard shots to 1.1keV when

$b^{1,-7}_{r,ref}(a)/B(a) = 0.5\%$ with few cases also above $1.2keV$; at larger values of the applied perturbations T_e is reduced for Deuterium too and returns below 1keV. The electron confinement time in panel c follows the T_e dependence on $b^{1,-7}_{r,ref}(a)/B(a)$ with a peak for Deuterium of about $1.5ms$ in presence of low amplitude perturbations ($\leq 0.5\%$). In Hydrogen discharges τ_E is always below $1.5ms$, the value typical of standard shots without 3D fields, but is further reduced of more than 50% when $b^{1,-7}_{r,ref}(a)/B(a) \geq 0.5\%$.

In conclusion, the application of a non zero external reference for the dominant mode, if kept at a low amplitude, can positively affect the eITB dynamic and confinement properties only in Deuterium plasmas while this does not occur in the hydrogen ones which are characterized by a general worsening of the main parameters. This represents a further beneficial outcome of using Deuterium -i.e. obtaining longer QSH thanks to the external fields - but with the same or partially improved performances with respect to spontaneous helical states in standard discharges. The different behavior between the two gas is still probably to be correlated with the edge physics; indeed as reported in the next section the main gas influx in H is $\sim 30 - 40\%$ greater than in D plasmas.

6. Isotope effect on particle confinement and influx

In RFX-mod the shape of density profiles changes from almost flat at low density to hollow at high density[17]. The hollowness of high density profiles has been related to the presence of an outward velocity greater than the inward $V_{E\times B}$ velocity. Interpretative analyses show that the total particle diffusion coefficient D_{tot} in Hydrogen plasmas is much higher in the core than the neoclassical diffusion coefficient D_{neo}, due to the contribution of an anomalous term D_S that accounts for the effect of magnetic field stochasticity [42]. In a stochastic magnetic field the particle flux is related to the density gradient through the particle diffusion D_S, and to the density itself through the outwardly directed velocity V_S, that sets up to equalize electron and ion outfluxes [43, 44]. The onset of V_S can explain the hollowness of profiles measured in high density plasma, which are characterized by a strong MHD turbulence in the core. Though the diffusivity in D is lower than in H, the stochastic channel remains the dominant core transport even in the purest QSH phases characterized by the development of ITB [17].

The core density in RFX-mod is measured with a double-wavelength vibration compensated interferometer [45] working in the mid-infrared range. The interferometer observes the plasma along 13 chords, whose normalized impact parameters h/a range from 0.1 to 0.93.

As a first guess of the profile shape the peaking factor P, a parameter equal to the time averaged central density normalized to the edge density, is considered. The central density $n_{central}$ is evaluated averaging the measurements of the two innermost chords (h=$\pm$ 0.05 m). The average value of the edge density n_{edge} is instead evaluated using the most external available chords that measure in the region external to 0.34 m

(h/a=0.74). Given these chords, P of a flat profile is equal to 1, P of a parabolic profile is equal to 2, while hollow profiles are found when P is lower than 1.

The plot of P average values shown in Fig. 19 shows that the density profile does not experience any isotope effect, since it maintains flat even in Deuterium. A deeper insight into the profile shape can be obtained applying an inversion algorithm to the interferometer measurements; the profiles shown in Fig. 20 are obtained applying such algorithm to the measurements at $n/n_G \sim 0.12$.

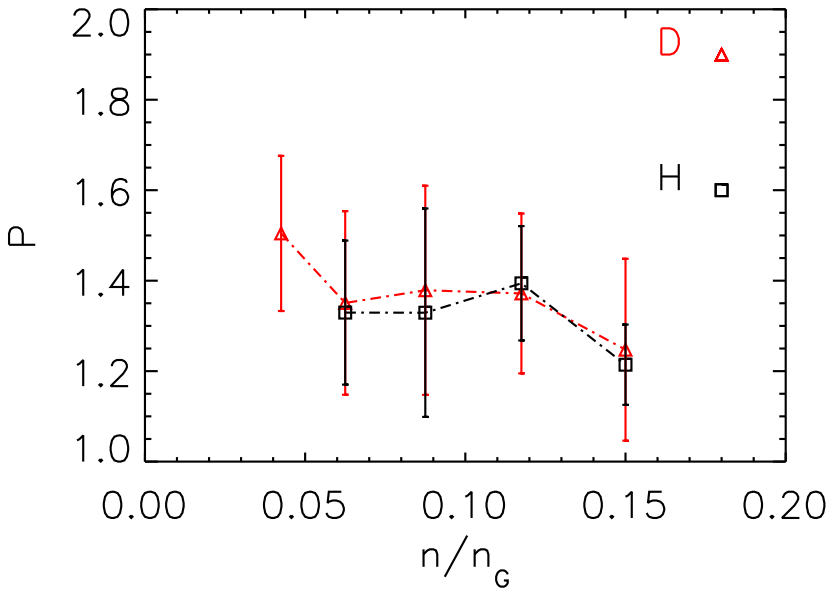

Figure 19. Comparison of peaking factor of density profile found in Hydrogen and Deuterium plasmas.

Such profiles are normalized in order to have the same value of central density, so that P follows the behaviour of the edge density: the lower the edge density the higher the P values.

The typical value of P in this class of density is about 1.4. As anticipated by the amplitude of error bars in Fig 19, in each class of density a significant variability of profile shape is observed: this is shown by the profiles plotted with lines in Fig. 20, which account for the extrema of the error bars on the peaking factor averages.

The profiles with the highest edge density have $P \sim 1.25$ while the remaining profiles, those with the lowest edge density, have $P \sim 1.5$. The comparison between D and H data confirm that the shape of density profile does not experience the isotope effect.

In RFX-mod the two diagnostics used to measure the density at the edge are the reflectometer [46] and the THB. Fig. 21 shows the values of the distance from the wall of the cut-off density layer with the density around $1{\cdot}10^{19}\mathrm{m}^{-3}$, averaged during the QSH phases. The graph, where the two curves relative to Hydrogen and Deuterium nearly

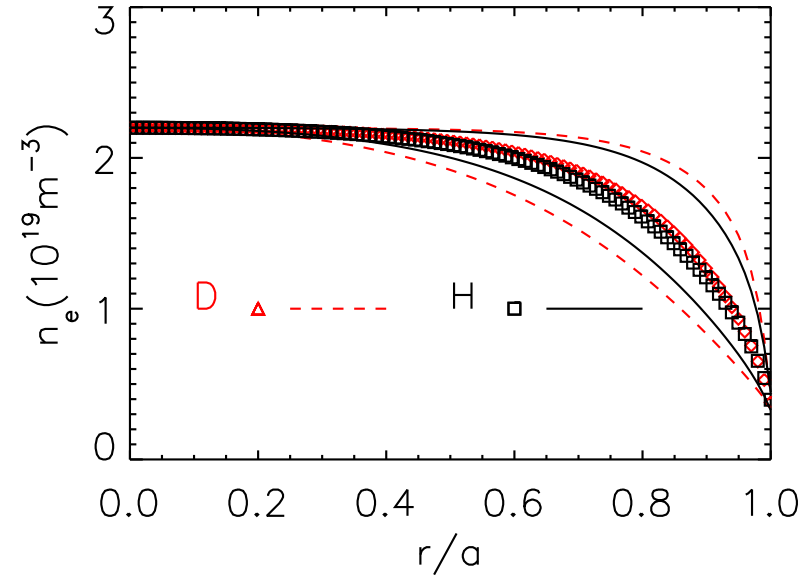

Figure 20. Density profiles in discharges at $n/n_G \sim 0.12$: the average shape of profiles is plotted with symbols while the lines show the profile variability

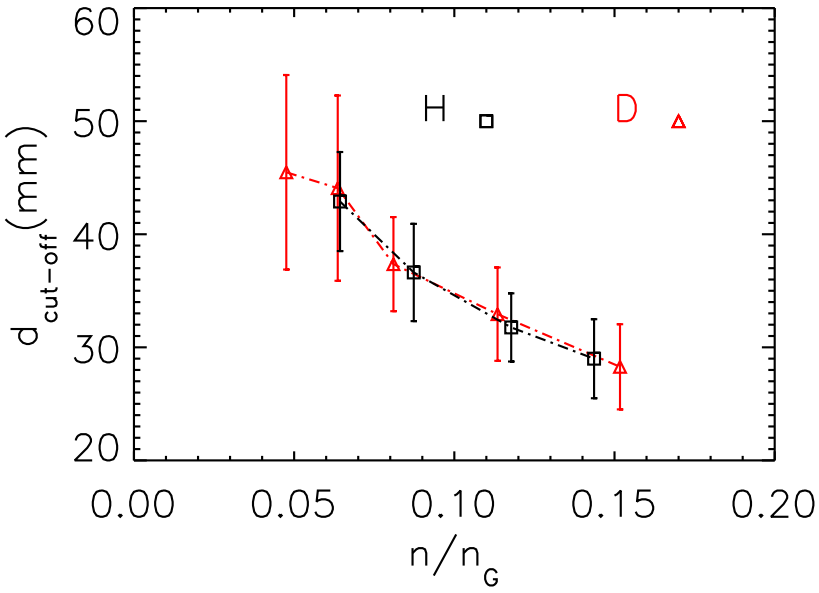

Figure 21. Comparison of the distance from the wall $d_{cut-off}$ of the density layer $1{\cdot}10^{19}m^{-3}$ in Deuterium and Hydrogen plasma.

overlap, confirms that, as it happens in the core, in the edge the density is insensitive to isotope mass M_i. Analogous results are provided by the data coming from the THB.

Such result confirm what already found in RFX when profiles of Hydrogen and

Helium plasma have been compared [48].

The theory of transport in a stochastic magnetic field says that the stochastic particle diffusion coefficient D_S scales as ${M_i}^{-0.5}$ and it is proportional to the energy of secondary modes. Hence D_S is expected to assume a lower value in Deuterium plasma than in Hydrogen plasma.

However simulations obtained with the Hamiltonian guiding center code ORBIT [49] show that the total particle diffusion coefficient $D_{tot} = D_{neo} + D_S$ is nearly invariant with M_i since the reduction of the stochastic term [50] balances the increase of neoclassical term D_{neo}.

The total velocity V_{tot} is the sum of the inwardly directed $V_{E\times B}$ and of the outwardly directed stochastic term V_S; the latter is usually found to dominate in RFX and RFX-mod [17, 42, 48] so that V_{tot} is outwardly directed. The lower stochasticity found in Deuterium, in the hypothesis of a weak depence of T_i on M_i, requires a lower V_S to balance the particle fluxes so that the sign of V_{tot} magnitude could even change.

Such considerations could lead us to conclude that the ratio V_{tot}/D_{tot}, that regulates the density gradient internally to the neutral penetration depth $r/a < 0.85$ (r < 0.4 m) [48], decreases moving from H to D, so that more peaked profile would be expected. However we cannot draw a definite conclusion on this subject since measurements of ion temperature, whose normalized gradient links D_S to V_S, were not available during the experiments.

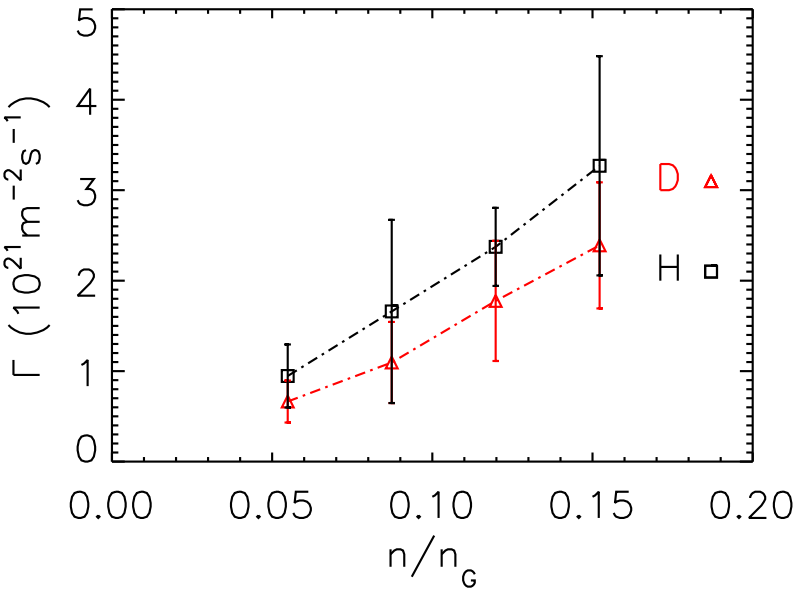

Figure 22. Comparison of particle influx in Hydrogen and Deuterium plasmas. Data are measured during QSH.

The plots of Deuterium and Hydrogen influxes [51] of Fig. 22 show that Hydrogen influxes are 30-40% higher than the Deuterium ones. This difference reflects in the

scaling law for the particle confinement time $\tau_p \sim M_i^{0.45}$, due to the invariance of the density profile shape. Such a scaling is weaker than that found in tokamak [35, 36], where $\tau_p \sim M_i$.

On the base of a one-dimensional approach for the particle balance we can infer some conclusions on particle transport at the edge. Simulations indicate that in the region external to $r/a = 0.85$, where strong density gradients and neutral particles coexist, the particle flux coincides with the diffusive one Γ_D. Therefore Γ_D balances the volume integral Γ_S of the particle source S, if the plasma is in a stationary condition. $S = n_n n_e \sigma_{ion}$ is the product of neutral density, electron density and the ionization rate σ_{ion} [48, 17].

The balance between Γ_S and Γ_D can be written in cylindrical geometry as:

$$\Gamma_S = \frac{\int_{V(r)} S(r) dV}{4\pi^2 R r} \sim \Gamma_D = D \frac{dn_e}{dr} \tag{4}$$

The term Γ_S calculated in Deuterium plasma is lower than in Hydrogen one, since it is proportional to the neutral density and, therefore to the particle influx. The balance between the two terms shown in Eq. 4, combined to the invariance of density gradients has as a consequence that the diffusion particle coefficient is lower in Deuterium than in Hydrogen. This result confirms that in RFPs the isotope effect occurs mainly at the edge, where the transport is driven by electrostatic fluctuations. Such observation of analogous density profile in different main gases shares many similarities with the results obtained in the RTP tokamak [52]. Interestingly the isotope effect in tokamaks, where it is mainly an edge effect too, has been explained by using ITG driven instability theory [53, 54, 55].

The impact of the helical geometry and of residual level of magnetic chaos due to secondary modes on the transport of ions with different mass has been investigated by means of the Hamiltonian guiding center code ORBIT [49] in its upgraded version [56, 57] which takes into account the non-axisymmetric shape of flux surfaces in the core of the plasma. The inputs for ORBIT are the Shafranov shifted axisymmetric equilibrium, computed by a $\mu\&p$ [58] model, and the radial profile of the eigenfunctions $b^r_{m,n}(r)$ relative to the (m, n) harmonics which can be reconstructed by using Newcomb equations [59] from the experimental values of the perturbed field measured at the edge of the plasma; in the simulations considered here: $m = 1, n = -7, -8, -9, ..., -15$. An example of magnetic field Poincaré map at the poloidal angle $\theta = 0$ from ORBIT is shown in the top panel of Fig. 23 relative to a RFX-mod QSH regime: a clear footprint of the $(1, -7)$ helical structure is visible in the region with $r/a = 0.2 - 0.5$ surrounded by magnetic chaos. Transport simulations have been performed by initially placing 500 mono-energetic test ions in the region of the eITB, with a random direction in the velocity. The energy of the particles correspond to $T_i = 0.7 T_e$ where T_e is the electron temperature in the center of the plasma; collisions are also implemented in the code (classical and pitch angle scattering) and their frequency is determined from T_e and the background density measurements.

Ions diffuse subjected to collisions and to the drifts induced by their energy and by

the magnetic field; the time required for half their population to reach the thick blue helical surface S_L in Fig.23a is named loss time τ_L. These runs have performed for a subset of the database analyzed in the previous sections, thus for both Hydrogen and Deuterium discharges. The resulting τ_L are plotted in the bottom panel of Fig. 23 vs $b_s/B(a)\%$ in red-diamonds for Deuterium and black-circles for Hydrogen. Loss times of the heavier isotope vary between 1.5 and $2.5ms$, while those of Hydrogen are always below 1.5ms, independently of applied helical boundary conditions. Very different values of τ_L might correspond to the same amplitude of the secondary modes (for instance at $b_s/B(a) \sim 0.52\%$) since $b_s/B(a)$ is only one of the parameter affecting the particle transport which depends also on the test ion energy implemented (determining the drift of the particles), on collisionality and finally on the phases of the secondary modes.

It is useful to consider the average loss time ratio between Deuterium and Hydrogen plasmas at the same level of residual chaos i.e. $b_s/B(a)\% \sim 0.65 - 0.82\%$ (region between the vertical dashed lines) which is $< \tau_{L,D}/\tau_{L,H} > \approx 1.28 \pm 0.05$. Such a value must be compared with the estimate in a full stochastic field where transport is dominated by the parallel thermal velocity, scaling with the inverse of the atom mass [43, 44]; in this regime, at the same energy, the particle diffusion coefficient D_p for Deuterium is expected to be lower than for Hydrogen by a factor $\sqrt{(M_H/M_D)} = 1/\sqrt{2}$ (assuming the same energy for both the gases).Since $\tau_L \propto 1/D_p$, in a chaotic domain $< \tau_{L,D}/\tau_{L,H} > \sim 1.41$ is expected. It is worth to note that the Larmor radius is mainly independent from the magnetic fluctuations level since they are about a factor 10^3 lower with respect to the equilibrium fields magnitude. On the contrary, in a pure helical geometry with conserved magnetic surfaces, where the neoclassical effects become more important, the particles diffusion is mostly determined by banana orbit and gyroradius dimensions which in Deuterium are larger than in Hydrogen by a factor of the order $\sqrt{(M_D/M_H)} \sim \sqrt{2}$; this would lead to $< \tau_{L,D}/\tau_{L,H} > \sim 0.71$. The result obtained in the simulations reported above highlights the peculiar field structure in the QSH regimes of RFX-mod which is characterized by a diffusion mechanism neither typical of a fully stochastic configuration neither of a pure helical topology. A partial confirmation of what obtained in the simulations come from the experimental results reported in [61] on Hydrogen diffusion coefficients which scale $(b_s/b_{1,-7})^{1.5}$ (see also [60]) and not with b_s^2 as expected for transport in a chaotic magnetic fields [43].

7. Conclusions

The results shown in this paper demonstrate that, as it happens for tokamaks, the RFP configuration experiences the isotope effect, at least when QSH states are considered. The isotope mass influences both the core and the edge of the plasma. The effect that the higher M_i has on tearing modes reminds the stabilizing effect of a closer shell. As a result the Deuterium QSHs are closer to the still theoretical Single Helicity state than the Hydrogen ones.

In detail, the higher M_i reduces the amplitude of secondary modes, while the

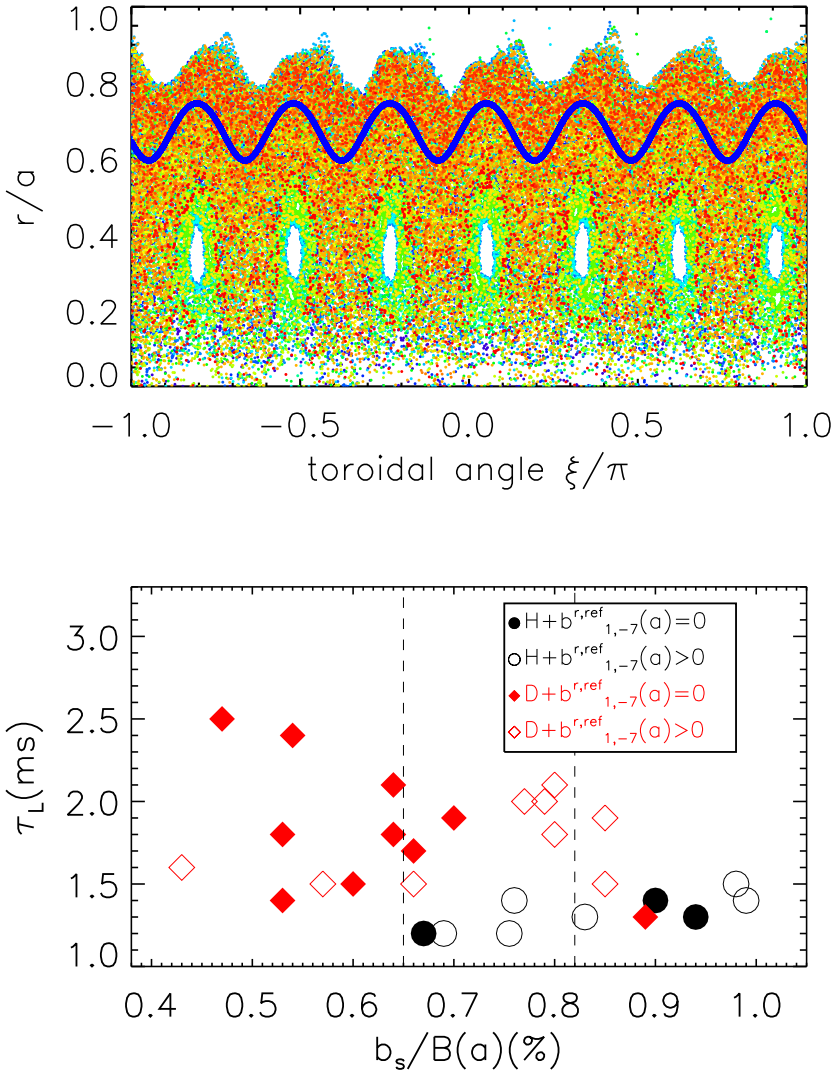

Figure 23. On the top: Poincaré plot on a toroidal section of Quasi Single Helicity state topology; on the bottom: helical loss time.

dominant mode is almost unaffected, so that the Quasi Single Helicity phases are purer. Furthermore, QSHs last longer, due to an increased resilience to small Dynamo Relaxation Events.

The increase of the main gas mass, replacing Hydrogen with Deuterium, has a beneficial effect on the plasma performances, as proved by the increase of both energy and particle confinement time.

The energy confinement time τ_E scales with the mass M_i of the isotope having the highest concentration as $\sim {M_i}^{0.3}$ while the particle confinement time τ_p follows a $\sim {M_i}^{0.45}$ scaling law. As a further result of such stabilization the core temperature gradients are steeper and the thermal structures typical of QSH are wider. However, the improvement

of core gradients by itself is not sufficient to explain the increase of the core electron temperature, which is mainly due to a steepening of the gradients at the plasma edge.

While the isotope effect in the core gradients is always lost during a DRE, the improvement of edge gradients survives the Dynamo Relaxation Events that do not bring the plasma to MH.

The improved resistance to perturbations of Deuterium plasma is confirmed by the application of low-amplitude 3D fields; as a result a worsening of the thermal properties in Hydrogen plasmas is observed, while the core temperature of Deuterium plasma remains unaffected. This gives the possibility of obtaining longer induced QSH with the same performances of spontaneous ones.

Even the scaling of τ_p with M_i is the result of an isotope edge effect, marked by the behaviour of the neutral influx.

The concluding remark is that, since the Deuterium discharges used in this paper are actually a mixture of Hydrogen and Deuterium, a stronger isotope effect will be found with a nearly pure Deuterium plasma.

References

[1] H.A.B. Bodin and A.A Newton. 1980 Nucl. Fusion 20 1255
[2] S. Ortolani and D.D. Schnack 1993 Magnetohydrodynamics of Plasma Relaxation (Singapore: World Scientific)
[3] J. Wesson Tokamaks 3rd edn (Oxford: Oxford University Press) (2004)
[4] P. Sonato *et al*, Fusion Engineering and Design **66**, 166 (2003)
[5] S. Peruzzo *et al*, Fus. Eng. and Des, 146, 692 (2019)
[6] L. Marrelli *et al*., Nucl. Fusion **59**, 076027 (2019)
[7] N. Vianello *et al*., Plasma Phys **58** 044099 (2016)
[8] C. Rea *et al*., Nucl. Fusion **55**, 113021 (2015)
[9] G. Spizzo *et al* Phys. Rev. Lett. 96 025001 (2006)
[10] Finn J.M. Finn, R. Nebel and C. Bathke 1992 Phys. Fluids B 4 1262
[11] S. Cappello and R. Paccagnella, Phys. Fluids B **4**, 611 (1992)
[12] P. Martin *et al*, Nucl. Fusion **43**, 1855 (2003)
[13] R. Lorenzini *et al* 2009 Nature Phys. 5 570
[14] R. Lorenzini *et al* Phys. Rev. Lett. **116**, 185002 (2016)
[15] P. Piovesan *et al*, Nucl. Fusion **49**, 085036 (2009)
[16] D. Terranova *et al*, Nucl. Fusion **50**, 035006 (2010)
[17] F. Auriemma *et al*, Nucl. Fusion **55**, 043010 (2015)
[18] D. F. Escande *et al*, Phys. Rev. Lett. **85**, 1662 (2000)
[19] R. Lorenzini *et al*, Nucl. Fusion 55 (2015) 043012
[20] M. Gobbin *et al*, Plasma Phys. Control. Fusion 57 (2015) 095004
[21] P. Zanca, L. Marrelli, G. Manduchi and G. Marchiori (2007) Nucl. Fusion 47 1425
[22] P. Zanca, Plasma Phys. Control. Fusion 51 015006 (2009)
[23] M. Valisa *et al*, Plasma Phys. Control. Fusion **50**, 124031 (2008)
[24] P. Scarin *et al*, Nucl. Fusion **51**, 073002 (2011)
[25] J. R. King *et al* et al., Phys. Plasmas **18**, 042303 (2011)
[26] R. Lorenzini *et al*, Nucl. Fusion **47**, 1468 (2007)
[27] N. Mattor *et al*, Phys. Plasmas **3**, 1578 (1996)
[28] K. Hattori *et al*, Phys. Fluids B **3**, 3111 (1991)
[29] R. N. Dexter *et al*, Fusion Technol. **19**, 131 (1991)

[30] A. Alfier and R. Pasqualotto, Rev. Sci. Instrum. **78**, 013505 (2007)
[31] M. Agostini *et al*, Rev. Sci. Instrum. **81**, 10D715 (2010)
[32] P. Franz *et al*, Nucl.Fusion **53**, 053011 (2013)
[33] R. Lorenzini *et al*, Nucl. Fusion **52**, 062004 (2012)
[34] A. Scaggion *et al*, Plasma Phys. Control. Fusion **56**, 015008 (2014)
[35] M. Bessenrodt-Weberpals *et al*, Nucl. Fusion **33**, 1205 (1993)
[36] U. Stroth *et al*, Plasma Phys. Control. Fusion **40**, 9 (1998)
[37] A. Murari *et al*, Rev. Sci. Instrum. **70** No.1 562 (1999)
[38] M. Gobbin *et al*, Phys. Rev. Letters **106**, 025001 (2011)
[39] P Piovesan et al 2011 Plasma Phys. Control. Fusion 53 084005
[40] L. Frassinetti *et al*., Nucl. Fusion **49** (2009) 075019
[41] P. Zanca *et al* Nucl. Fusion **47** 1425 (2007)
[42] D. Gregoratto *et al*, Nucl. Fusion **38**, 1199 (1998)
[43] A. B. Rechester and M. N. Rosenbluth, Phys. Rev. Lett. **40**, 38 (1978)
[44] R. W. Harvey *et al*, Phys. Rev. Lett. **47**, 102 (1981)
[45] P. Innocente *et al*, Rev. Sci. Instrum. **68**, 694 (1997)
[46] G. De Masi *et al*, Nucl. Fusion **53**, 083026 (2013)
[47] G. De Masi *et al*, Nucl. Fusion **51**, 053016 (2011)
[48] R. Lorenzini *et al*, Phys. Plasmas **13**, 112510 (2006)
[49] R. B. White and M. S. Chance, Phys. Fluids **27**, 2455 (1984)
[50] M. Gobbin *et al*, Proc. 25th Eur. Conf. on Controlled Fusion and Plasma Physics (Berlin) (2014)
[51] L. Carraro *et al*, Rev. Sci. Instrum. **66**, 610 (1995)
[52] B. H. Deng *et al*, Phys. Plasmas **8**, 2163 (2001)
[53] J. Q. Dong *et al*, Phys. Plasmas **1**, 3635 (1994)
[54] W. W. Lee *et al*, Phys. Plasmas **4**, 169 (1997)
[55] R. R. Dominguez *et al*, Nucl. Fusion **31**, 2063 (1991)
[56] M. Gobbin, L.Marrelli, P.Martin and R.B.White, Phys. Plasmas **14** 072305 (2007).
[57] M. Gobbin *et al*, Plasma Physics Control. Fusion **51** 065010 (2009)
[58] H.A.B. Bodin and A.A. Newton 1980 Nucl. Fusion **20 1255**
[59] P.Zanca and D. Terranova, Plasma Phys. Control. Fusion 46, 1115-1141, (2004).
[60] F. DÁngelo et R. Paccagnella, Plasma Phys. Control. Fusion 41 941 (1999)
[61] K. Behringer *et al* **Plasma Phys. Control. Fusion 31 2059 (1989)**